Z. Kristallogr. 217 (2002) 581–590

Structural and chemical variations in rathite, $Pb_8Pb_{4-x}(Tl_2As_2)_x(Ag_2As_2)As_{16}S_{40}$: modulations of a parent structure

P. Berlepsch*, I, Th. Armbruster[I] and D. Topa[II]

[I] Universität Bern, Laboratorium für chemische und mineralogische Kristallographie, Freiestrasse 3, CH-3012 Bern, Switzerland
[II] Universität Salzburg, Departement für Geologie und Mineralogie, Hellbrunner Str. 34/III, A-5020 Salzburg, Austria

Received December 3, 2001; accepted June 5, 2002

Abstract. Members of the 4,4 sartorite homologues can be deduced from a topological parent structure with orthorhombic symmetry, space group *Pmnb*, $a = 4.233$, $b = 7.918$, $c = 24.692$ Å. The observed modulations in 4,4 sartorite homologues are associated with symmetry lowering of the parent structure and superstructure formation. The Pb, Tl, Ag, As, Sb sulfosalt rathite is a 4,4 member of the sartorite homologous series with space group symmetry $P2_1/c$ and is isostructural to synthetic $Ba_{12}Sb_{18.64}S_{40}$ and closely related to $Ba_{10.48}Pb_{5.52}Sb_{16}S_{40}$ of reduced symmetry $P2_1$. In these structures the two-fold screw axes run parallel to b of the parent structure. Isotopological is also dufrénoysite $Pb_{16}As_{16}S_{40}$, another 4,4 homologue of the same series, of space group symmetry $P2_1$. In dufrénoysite, however, the two-fold screw axes run parallel to c of the parent structure. To elucidate the modulation of the parent structure, rathite has been structurally and chemically reinvestigated emphasising cation order/disorder relations. Single crystal X-ray structure refinement (space group $P2_1/c$; $a = 8.496(1)$, $b = 7.969(1)$, $c = 25.122(3)$ Å, $\beta = 100.704(2)°$; $R_1 = 3.67\%$ for 2718 reflections with $I > 2\sigma[I]$) yielded three split cation positions indicating heterovalent substitutions. Considering that isoelectronic Pb^{2+} and Tl^+ cannot be distinguished in our diffraction experiment the chemical composition $(Pb_{9.25}Tl_{1.37})_{\Sigma=10.62}Ag_{2.01}(As_{19.09}Sb_{0.83})_{\Sigma=19.92}S_{40}$ derived from electron microprobe analyses matches the formula $Pb_{10.96}Ag_{1.90}(As_{18.09}Sb_{1.06})_{\Sigma=19.15}S_{40}$ obtained from the structure refinement. The complex composition is caused by two independent heterovalent substitutions $Ag^+ + As^{3+} \rightarrow 2\,Pb^{2+}$ and $Tl^+ + As^{3+} \rightarrow 2\,Pb^{2+}$ leading to the simplified rathite formula $Pb_8Pb_{4-x}(Tl_2As_2)_x(Ag_2As_2)As_{16}S_{40}$. The substitution involving Ag seems to be essential for the formation of rathite and distinguishes rathite from dufrénoysite $Pb_{16}As_{16}S_{40}$. The Tl substitution in rathite appears to be optional. In addition, minor Sb^{3+} may replace As^{3+}.

Introduction

Baumhauer (1896) described rathite as a new mineral from the Lengenbach deposit (Binntal, Valais, Switzerland) and also reported its chemical composition as antimony-containing lead-arsenic sulfide with traces of iron. Nowacki and Bahezre (1963) detected the presence of some thallium in this mineral. The crystal structure of rathite was solved and refined by Marumo and Nowacki (1965). A careful re-determination of the chemical composition of rathite by Burri (in: Marumo and Nowacki, 1965) showed the presence of silver and accordingly Marumo and Nowacki (1965) defined the formula of rathite as $Pb_{11.1}Tl_{0.9}As_{16}(As_{1.6}Ag_{2.3})S_{40}$. Notice, however, this formula is not charge balanced yielding 77.3 positive charges with accounting As as trivalent and Ag as monovalent.

There exists a number of so-called rathite varieties, e.g., rathite-I and -II of Berry (1953), rathite-I, -II, and -III of Le Bihan (1962) or rathite-Ia and rathite-IV (Nowacki, Marumo and Takéuchi, 1964) as well as others, which keep on causing confusion. Choi and Kanatzidis (2000), for instance, define a group of rathite minerals to which they count rathite-I, rathite-Ia, rathite-III, and dufrénoysite. Some of these names should not be used any longer since their identity with previously described minerals has been shown meanwhile. A first attempt of 'cleaning' the group was made by Makovicky (1985, his Table 3) and the name rathite group should be avoided because there exists the sartorite homologous series, a supergroup of the above 'rathite group' (Makovicky, 1985). For these reasons it seemed worth to compile the different rathite varieties and attribute the correct names that are valid at present (Table 1).

On a modular structural level rathite is a 4,4 homologue of the sartorite homologous series of minerals (Makovicky, 1985). Other 4,4 member of the same series are dufrénoysite $Pb_{16}As_{16}S_{40}$, a pure lead-arsenic sulfosalt, veenite $Pb_{16}(Sb,As)_{16}S_{40}$ (Jambor, 1967), a structurally insufficiently well described Sb analogue of dufrénoysite, and the synthetic compounds $Ba_{12}Sb_{18.64}S_{40}$ (= $4 \times Ba_3Sb_{4.66}S_{10}$) and $Ba_{10.48}Pb_{5.52}Sb_{16}S_{40}$ (= $4 \times Ba_{2.62}Pb_{1.38}Sb_4S_{10}$) of Choi and Kanatzidis (2000). Rathite and dufrénoysite are known to form exsolution intergrowths.

The crystal chemistry of sartorite homologues was worked out by Nowacki's school (e.g., Iitaka and Nowacki, 1961; Nowacki et al., 1961), by the comparative analysis of Makovicky (1985), and by the coordination analysis of Berlepsch, Makovicky, and Balić-Žunić (2001).

---

* Correspondence author (peter.berlepsch@krist.unibe.ch)

Table 1. Selected rathite varieties reported in literature and their correct names.

Rathite variety reported in literature		in fact is	
Rathite	Baumhauer (1896)	Rathite	
α-Rathite	Solly	Rathite	Solly (1911)
Rathite-I	Berry (1953)	Rathite	
Rathite-II	Berry (1953)	Liveingite	Nowacki (1967); Engel and Nowacki (1970)
Rathite-I	Le Bihan (1962)	Dufrénoysite	Marumo and Nowacki (1965)
Rathite-II	Le Bihan (1962)	Liveingite	Nowacki (1967)
Rathite-III[a]	Le Bihan (1962)		
Rathite-1a[b]	Nowacki and Bahezre (1963)	Dufrénoysite	Nowacki and Bahezre (1963)
Rathite-IV	Nowacki et al. (1964)	Sartorite	Nowacki et al. (1964)
Rathite-V	Nowacki et al. (1964)	Rathite-IV[c]	Ozawa and Nowacki (1974)

a: We consider the structure solution of rathite-III as erroneous. It cannot simply be derived from the *Pnmb* parent structure (Table 4) although the cell dimensions of rathite III are similar to the parent structure with the difference that the *a*-axis of rathite-III is doubled.
b: Since Berry (1953) was the first who used the names rathite-I and rathite-II Nowacki and Bahezre (1963) decided to rename Le Bihan's rathite-I into rathite-1a.
c: Rathite-V was renamed rathite-IV after rathite-IV became identical with sartorite.

Pring (2001) unravelled the complex HRTEM architecture of the sartorite group. Makovicky (1985) proposed an aristotype (parent structure) with *Pbnm* symmetry for sartorite homologues and Pring (2001) defined the dimensions of a so called topological parent structure for 4,4 homologues by a cell of orthorhombic symmetry ($a_p = 4.2$ Å, $b_p = 7.9$, $c_p = 24.7$ Å) which, for the true structure, becomes doubled parallel to a_p and c_p leading to a *B*-centred pseudo-orthorhombic cell and hence can be transformed into the conventional primitive monoclinic setting. In addition, Pring (2001) emphasized the well ordered nature of rathite TEM images and displayed sharp electron diffraction patterns without any diffusiveness in agreement with the monoclinic cell. There was no indication of polytypism or polysomatic disorder.

During a routine check of mineral samples from the Lengenbach deposit (Valais, Switzerland) rathite has been identified. The relatively high R_1-value of 8.6% for the refinement of the crystal structure of rathite (Marumo and Nowacki, 1965) based upon integrated film data and uncertainties regarding the exact chemical composition of rathite made it worth to revise both the chemical and crystallographical data of rathite. The results of new electron microprobe analyses and a structure refinement are presented in this study. The structure of rathite is compared on a modular level as well as on the basis of $(100)_{\mathrm{SnS}}$ layers to those of dufrénoysite, $\mathrm{Ba_{12}Sb_{18.64}S_{40}}$ and $\mathrm{Ba_{10.48}Pb_{5.52}Sb_{16}S_{40}}$. Super- and subgroup relationships between the four topologically identical compounds are discussed.

Sample description

The fragments used for structural and chemical work are black and have dark red internal reflections and originate from a larger aggregate that grew hydrothermally in a druse within white dolomite rock. Rathite in this sample is associated with pyrite and tennantite. The various morphologies and relative crystal sizes of rathite suggest that rathite formed (a) tiny needles in an early stage of growth. These needles flattened into (b) small lathlike crystals in a later stage of growth. Towards the final stage of growth (c) larger prismatic crystals or crystal aggregates formed. All morphologies (a)–(c) are observed on the specimen from which two crystal fragments of type (c) were used for chemical analyses and one crystal of type (b) was used for single crystal X-ray diffraction analyses. These choices reflect the most appropriate crystal sizes for the respective experiments.

Experimental procedures

Chemical analyses

Quantitative chemical analyses were performed on a JEOL JXA-8600 electron microprobe (EMP), controlled by a LINK-*eXL* system, operated at 25 kV, 35 nA, and 20 s counting time for peaks and 7 s for background, and a beam diameter of 5 µm. The following standards and X-ray lines were used: galena (PbS: PbM_α, SK_α), nickeline (NiAs: AsL_α), Ag metal (AgL_α), stibnite ($\mathrm{Sb_2S_3}$: SbL_α), lorandite ($\mathrm{TlAsS_2}$: TlL_α), chalcopyrite ($\mathrm{CuFeS_2}$: FeK_α, CuK_α). Raw data were corrected with the on-line ZAF-4 procedure and the results are listed in Table 2. Backscattered electron (BSE) images of the analysed samples show grain 1 to be homogeneous. In the matrix (m) of grain 2 some darker (d) and brighter (b) zones are observed in the BSE images. In Table 2 the sets of chemical data related to these zones are labelled 2m, 2d, and 2b, respectively. The measured Fe in crystal 1 results most probably from pyrite ($\mathrm{FeS_2}$) inclusions in the analysed rathite, although already Baumhauer (1896) reported traces of Fe in rathite.

The number of rathite analyses and the variations in chemical composition are too small to establish any firm regression lines for chemical substitutions. However, with eight symmetry independent cation sites occupied solely by Pb and As, the only charge balanced compound is $\mathrm{Pb_4As_4S_{10}}$ (i.e., the composition of dufrénoysite) and departure from this composition is achieved according to the equation $(\mathrm{As, Sb})^{3+} + (\mathrm{Ag, Tl})^{+} \rightarrow 2\,\mathrm{Pb}^{2+}$ (Makovicky, 1985, his Figure 13). Replacement of $6\,\mathrm{Pb}^{2+}$ by $2\,\mathrm{As}^{3+}$, $1\,\mathrm{Sb}^{3+}$, $2\,\mathrm{Ag}^{+}$, $1\,\mathrm{Tl}^{+}$ leads to a charge balanced formula that is very close to those derived from structural and

Table 2. Chemical composition of rathite from Lengenbach deposit.

Crystal	N.A.	Pb wt%	Tl wt%	As wt%	Sb wt%	Ag wt%	Fe wt%	S wt%	Sum wt%
1	9	39.49	3.49	25.68	2.95	4.18	0.08	24.50	100.37
2d	3	36.62	5.10	26.85	2.42	4.04		24.77	99.80
2b	3	38.51	4.41	26.59	2.05	3.86		24.31	99.74
2m	11	36.61	5.36	27.31	1.94	4.13		24.48	99.82
Formulae normalized on 40 S atoms pfu									
1	9	9.98(33)	0.89(12)	17.94(14)	1.27(14)	2.03(5)	0.07(4)	40.00	
2d	3	9.15(8)	1.29(2)	18.55(9)	1.03(2)	1.94(4)		40.00	
2b	3	9.80(9)	1.14(7)	18.77(8)	0.89(6)	1.89(3)		40.00	
2m	11	9.25(8)	1.37(2)	19.09(11)	0.83(4)	2.01(3)		40.00	

N.A. = number of analyses; d = dark; b = bright, m = matrix

1	$(Pb_{9.98}Tl_{0.89})_{\Sigma\,10.87}$	$Ag_{2.03}(As_{17.94}Sb_{1.27})_{\Sigma\,19.21}$	S_{40}	this study (EMP data)
2d	$(Pb_{9.15}Tl_{1.29})_{\Sigma\,10.44}$	$Ag_{1.94}(As_{18.55}Sb_{1.03})_{\Sigma\,19.58}$	S_{40}	
2b	$(Pb_{9.80}Tl_{1.14})_{\Sigma\,10.94}$	$Ag_{1.89}(As_{18.77}Sb_{0.89})_{\Sigma\,19.66}$	S_{40}	
2m	$(Pb_{9.25}Tl_{1.37})_{\Sigma\,10.61}$	$Ag_{2.01}(As_{19.09}Sb_{0.83})_{\Sigma\,19.92}$	S_{40}	
	$Pb_{10.96}$	$Ag_{1.90}(As_{18.09}Sb_{1.06})_{\Sigma\,19.15}$	S_{40}	this study (structure refinement)
	$(Pb_{11.1}Tl_{0.9})_{\Sigma\,12.0}$	$Ag_{2.3}\ As_{17.6}$	S_{40}	Marumo and Nowacki (1965)
	$(Pb_{11.36}Tl_{0.36})_{\Sigma\,11.72}$	$Ag_{1.88}(As_{19.10}Sb_{0.14})_{\Sigma\,19.24}$	S_{40}	Laroussi et al. (1989)
	$(Pb_{11.48}Tl_{0.27})_{\Sigma\,11.75}$	$Ag_{1.67}\ As_{17.95}$	S_{40}	Graeser unpublished (in: Pring, 2001)

EMP analyses (Table 2). Compared to the analyses of Laroussi, Moëlo, Ohnstetter, and Ginderow (1989) as well as those of Graeser (in: Pring, 2001) our rathite analyses display less Pb and more Tl with an almost constant value of about 2 Ag pfu.

Single crystal X-ray diffraction

A lathlike crystal of rathite, about 0.03 × 0.05 × 0.23 mm^3 in size, was measured on a Bruker AXS three-circle diffractometer (equipped with a CCD 1000 K area detector and a flat graphite monochromator) using MoK_α X-radiation from a fine focus sealed tube (Table 3). A SMART system of programs (Bruker AXS, 1998) was used for crystal lattice determination and X-ray data collection and SAINT+ (Bruker AXS, 1999) for the data reduction including intensity integration, background and Lorentz-polarization corrections. The program XPREP (Bruker AXS, 1997) was used for empirical absorption correction based on pseudo ψ-scans. The centrosymmetric space group $P2_1/n$, proposed by the program XPREP (Bruker AXS, 1997), was chosen consistent with the monoclinic symmetry of lattice and intensity statistics ($|E^2 - 1| = 0.991$). The space group $P2_1/n$ was subsequently transformed by the matrix $\mathbf{R} = (1\ 0\ 0,\ 0\ {-1}\ 0,\ {-1}\ 0\ {-1})$ into standard setting $P2_1/c$ (Table 4).

Structure determination and refinement

The structure was solved by direct methods (program SHELXS by Sheldrick, 1997a) that revealed most of the cation positions. In subsequent refinement cycles (program SHELXL by Sheldrick, 1997b) additional cation and the S positions were deduced from the difference Fourier syntheses by selecting from among the strongest maxima at appropriate distances. Subsequently three split cation positions were localized. Cation attribution to these sites was guided by an analysis of M–S bond lengths, refinement of individual site occupancies, and the knowledge of the chemical composition based upon the EMP data. However, Tl did not enter the structure refinement since it cannot be distinguished from Pb with the experimental conditions used. The distinction between Ag and Sb is questionable and is discussed below. The final refinement was performed with anisotropic displacement parameters for all positions (except for M6b that is a low-populated As position close to Pb, cf. Table 5) and an empirical extinction coefficient. The occupancies of the split sites were refined allowing for Sb/As (M3), Ag/As (M5), and Pb/As

Table 3. Data collection and refinement parameters of rathite.

Diffractometer	Siemens CCD system
X-ray radiation	fine focus sealed tube, MoK_α
X-ray power	50 kV, 40 mA
Temperature	293 K
Detector to sample distance	5.439 cm
Maximum 2θ	56.08°
Resolution	0.75 Å
Rotation width	0.3°
Total number of frames	2082
Frame size	512 × 512 pixels
Measuring time per frame	120 seconds
Measured reflections	15866
Index range	$-11 \leq h \leq 11$; $-10 \leq k \leq 10$; $-32 \leq l \leq 32$
Observed reflections	15291
Unique reflections	3811
Reflections > $2\sigma(I)$	2718
R_{INT}	6.89%
R_σ	5.81%
Number of l.s. parameters	189
GooF	0.985
R_1, $F_o > 4\,\sigma(F_o)$	3.67%
R_1, all data	5.86%
wR_2 (on F_o^2)	8.94%

$R_{\mathrm{INT}} = \sum |F_o^2 - F_o^2\ (\mathrm{mean})| / \sum F_o^2$

$R_\sigma = \sum \sigma(F_o^2) / \sum F_o^2$

$R_1 = \sum ||F_o| - |F_c|| / \sum |F_o|$

$wR_2 = \{(\sum w[F_o^2 - F_c^2]^2 / \sum w[F_o^2]^2)\}^{1/2}$

$\mathrm{Goof} = \{(\sum w[F_o^2 - F_c^2]/[n - p])\}^{1/2}$

$w = 1/(\sigma^2[F_o^2] + [0.0426 \cdot \mathrm{P}]^2)$

$P = (\max\ (F_o^2, 0) + 2F_c^2)/3$

Table 4. Selected unit cell parameters of 4,4 sartorite homologues.

Compound	*a* (Å)	*b* (Å)	*c* (Å)	angle (°)	S.G.	Ref.
B-centred supercell	8.496	7.969	49.377	γ 90.97		[1]
Parent structure	4.233	7.918	24.692		*Pmnb*	[1]
Rathite	8.496(1)	7.969(1)	25.122(3)	β 100.704(2)	$P2_1/c$	[1]
Rathite	8.496(1)	7.969(1)	24.980(3)	β 98.918(2)	$P2_1/n$	[1]
Rathite	8.47(1)	7.94(1)	25.16(2)	β 100.47(16)	$P2_1/c^a$	[2]
$Ba_{12}Sb_{18.64}S_{40}$	8.955(2)	8.225(2)	26.756(5)	β 100.29(3)	$P2_1/c$	[3]
$Ba_{10.48}Pb_{5.52}Sb_{16}S_{40}$	8.8402(2)	8.2038(2)	26.7623(6)	β 99.488(1)	$P2_1$	[3]
Dufrénoysite	7.90(1)	25.74(4)	8.47(4)	β 90.35(12)	$P2_1$	[4]

S.G. = space group; Ref. = reference

a: S.G. transformed from $P2_1/a$ into standard setting $P2_1/c$.

[1] this study; [2] Marumo and Nowacki (1965); [3] Choi and Kanatzidis (2000); [4] Ribár et al. (1969).

Table 5. Site labels with element allocations, occupancy factors, fractional atomic coordinates and equivalent isotropic displacement parameters for rathite.

Site label	Atom type	Site occupancy	Original^a site labels	x/a	y/b	z/c	U_{iso}
Pb1	Pb	1	Pb1	0.47494(5)	0.75704(5)	0.205583(17)	0.04036(15)
Pb2	Pb	1	Pb2	0.98078(5)	0.74922(6)	0.20540(2)	0.05976(18)
M1	As	1	As1	0.29987(10)	0.85369(12)	0.34169(4)	0.0274(2)
M2	As	1	As2	0.24640(12)	0.33506(12)	0.14689(4)	0.0311(2)
M3a^b	Sb	0.265(9)		0.6884(12)	0.6243(14)	0.0380(4)	0.066(3)
M3b	As	0.735(9)	As3	0.6847(5)	0.6605(5)	0.0417(2)	0.0437(10)
M4	As	1	As4	0.13800(10)	0.67143(12)	0.05873(4)	0.0276(2)
M5a	Ag	0.474(10)	As5a	0.4162(3)	0.0111(4)	0.0772(2)	0.0448(10)
M5b	As	0.526(10)	As5b	0.4257(3)	0.0252(4)	0.0510(3)	0.0352(8)
M6a	Pb	0.739(4)	Pb3	0.90270(12)	0.08494(16)	0.07178(3)	0.0379(3)
M6b^c	As	0.261(4)		0.8732(11)	0.0374(14)	0.0780(4)	0.075(4)
S1	S	1	S1	0.2564(3)	0.9974(3)	0.26341(10)	0.0313(5)
S2	S	1	S2	0.2476(3)	0.4798(3)	0.22331(9)	0.0274(5)
S3	S	1	S3	0.5068(2)	0.6830(3)	0.32623(9)	0.0262(5)
S4	S	1	S4	0.9017(3)	0.1712(3)	0.17828(10)	0.0321(5)
S5	S	1	S5	0.6976(3)	0.8377(3)	0.11176(9)	0.0291(5)
S6	S	1	S6	0.1656(3)	0.8802(3)	0.12022(10)	0.0320(5)
S7	S	1	S7	0.3641(3)	0.5211(3)	0.09716(9)	0.0289(5)
S8	S	1	S8	0.9572(3)	0.5086(3)	0.08998(12)	0.0404(6)
S9	S	1	S9	0.5888(3)	0.1974(3)	0.01482(12)	0.0434(7)
S10	S	1	S10	0.1794(3)	0.1800(3)	0.01016(10)	0.0321(5)

a: The original site labels refer to the structure refinement of rathite by Marumo and Nowacki (1965)

b: Split position assumed but not refined by Marumo and Nowacki (1965)

c: New split position (this study).

(M6) summing to full occupancy. The highest residual peak was 2.56 e/Å^3, 0.78 Å from Pb2 and the deepest hole −1.96 e/Å^3, 0.91 Å from Pb2 at the end of the refinement. The refinement was stopped when the mean shift/esd for varied parameters dropped below 1%.

According to Marumo and Nowacki (1965) rathite usually is polysynthetically twinned. Possible pseudo-merohedral twinning (Herbst-Irmer and Sheldrick, 1998) of rathite is related to the existence of higher metric symmetry as evidenced by a *B*-centred pseudo-orthorhombic cell of $a = 8.496$, $b = 7.969$, $c = 49.377$ Å, $\gamma = 90.97°$ (Table 4). To test for such pseudo-merohedral twinning according to the twin law $\mathbf{R} = (-1\ 0\ 0,\ 0\ -1\ 0,\ 1\ 0\ 1)$ some refinements with the TWIN command (program SHELXL by Sheldrick, 1997b) have been made but showed that the investigated crystal fragment of rathite is untwinned. Fractional atomic coordinates are listed in Table 5. The labelling scheme is slightly modified from the one by Marumo and Nowacki (1965) but a comparison has been made in Table 5. Anisotropic displacement parameters are listed in a deposited Table. Since the crystal structure of rathite has already been discussed on a polyhedral level (Marumo and Nowacki, 1965) and due to unresolved S positions around the split cation sites bond distances and angles are not tabled in the present study.

Results and discussion

The rathite structure

The crystal structure of rathite is shown in Fig. 1 and some structural aspects have been marked. Rathite belongs to the sartorite homologues, a series of Pb–As sulfosalts with zigzag walls composed of columns of 'standing' tricapped trigonal coordination prisms of Pb (coordination number 9). The walls alternate with variously thick slabs composed of 'lying' monocapped trigonal coordination prisms of As and Pb (coordination number 7); these slabs are based on the SnS-archetype (Fig. 1). There exists a series of closely related compounds, e.g., Tl–As–Sb or Ba–Sb sulfosalts. The structure of the sartorite homolo-

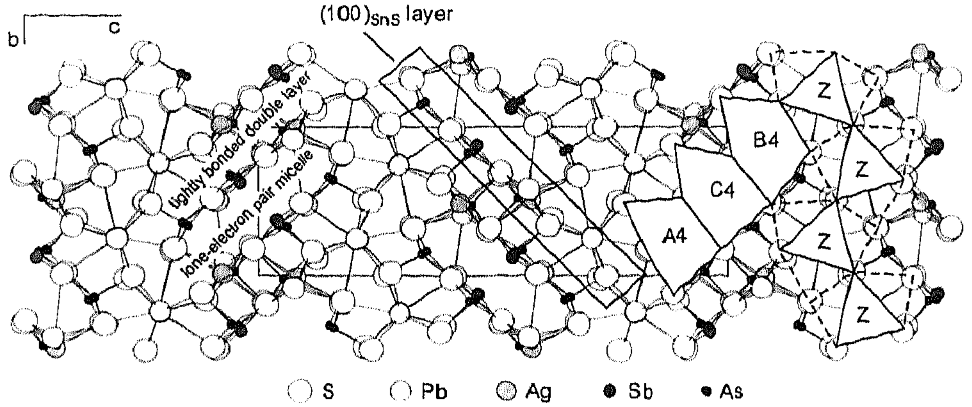

Fig. 1. The crystal structure of rathite projected along a. The polyhedral labelling scheme for sartorite homologues according to Berlepsch et al. (2001) is indicated. A $(100)_{SnS}$ layer, as displayed in figures 2, and 4–6 in views normal to the planes, is outlined.

gues can be visualized as composed of slices of SnS-like structure cut parallel to the planes $(301)_{SnS}$ or $(30\bar{1})_{SnS}$ (e.g., Fig. 9 in: Makovicky, 1997). These slices include polyhedra from both the walls and the slab and they are $N = 3$ to 4 polyhedra thick (Makovicky, 1985).

According to the labelling scheme for coordination polyhedra in sartorite homologues introduced by Berlepsch et al. (2001) Z denotes 'standing' tricapped trigonal coordination prisms in the zigzag walls whereas AN, BN, CN denote 'lying' monocapped trigonal coordination prisms within the slabs (with $N = 3$ or 4; Fig. 1). Rathite is a $N_{1,2} = 4,4$ member of the sartorite homologous series with Z hosting Pb and $A4$-$C4$ hosting As, Sb, Ag, and Pb (details are discussed below).

The refined structure of rathite corresponds basically to the structure model defined by Marumo and Nowacki (1965) but differs in details. Compared to Marumo and Nowacki (1965) our structure model contains two additional split cationic positions (M3 and M6). Marumo and Nowacki (1965) had one such split position labelled As5a and As5b. Based upon bond lengths the authors assumed that the As5a site actually hosts Ag and not As. Our refinement confirms this assumption. The M5a site in this study bonds to six S atoms between 2.73 and 2.84 Å and was refined as occupied by Ag (Table 5) whereas M5b has three closest S neighbours between 2.26 and 2.48 Å suggesting As. The additional split positions M3 and M6 split into partly occupied Sb (M3a), As (M3b) and Pb (M6a), As (M6b) positions (Table 5). M3a (Sb) has three shortest bonds to S between 2.38 and 2.58 Å whereas M3b (As) shows two short bonds to S5 (2.24 Å) and S10 (2.28 Å) and two longer additional bonds to S8 (2.69 Å) and S9 (2.73 Å). M6a (Pb) has six bonds to S between 2.76 and 3.14 Å whereas M6b (As) has five bonds to S between 2.44 and 2.93 Å (note that unresolved S positions influence these bond distances). The coordination of M6b is not characteristic of As but this site is only 26% occupied and associated S disorder could not be resolved. The strongest anisotropies of sulfur atomic displacement parameters were found for S8 and S9 both of which are associated with split cation positions. S8 bonds to M3a (Sb), M3b (As) and S9 bonds to all three split positions. Marumo and Nowacki (1965) mentioned that As3 has very large and anisotropic displacement parameters with the elongation of the thermal ellipsoid subparallel to the line S9–As3–S8 (corresponding to S9–M3–S8 in Fig. 2). A detailed bond-lengths analysis of M–S distances in the sartorite homologues suggested As3 in rathite (of Marumo and Nowacki, 1965) to be an unresolved superimposed position (Berlepsch et al., 2001). It is most interesting to see that our refinement indeed shows a split position M3 (Fig. 2).

It may be argued that the M3a site hosts Ag instead of Sb. However, the analysis of M–S bond lengths is ham-

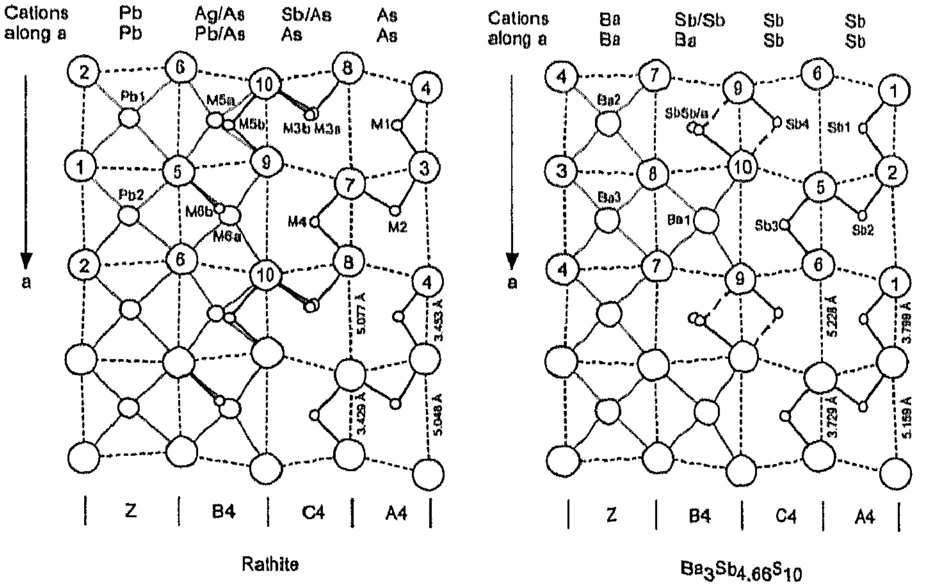

Fig. 2. $(100)_{SnS}$ layers in rathite and $Ba_{12}Sb_{18.64}S_{40}$, respectively. The dashed fine lines underline the trapezoidal arrangement of the S atoms. Short As–S and Sb–S bonds (bold lines) form the crankshaft chains in these layers (see text for details).

pered by unresolved S disorder depending on the kind and concentration of the central cation. In addition, the match between the chemical formula derived from EMP analyses (Table 2) and the one obtained from the structure refinement is better if Sb is assumed for the site M3a.

Among the sartorite homologues *sensu stricto* rathite and dufrénoysite are the only structurally sufficiently well described 4,4 homologues. They can occur in nature as exsolution intergrowths (Makovicky, 1985) and the question arises why two chemically similar compounds have closely related crystal structures with the one of rathite being centrosymmetric (space group $P2_1/c$) and the one of dufrénoysite being acentric (space group $P2_1$)? In addition, the two mineral structures have the two-fold screw axes oriented along different directions (Table 4). This question becomes even more interesting regarding similar findings for $Ba_{12}Sb_{18.64}S_{40}$ (space group $P2_1/c$) and $Ba_{10.48}Pb_{5.52}Sb_{16}S_{40}$ (space group $P2_1$), two 4,4 sartorite homologues *sensu largo* with orientations of the two-fold screw axes (Table 4) according to rathite (Choi and Kanatzidis, 2000).

Derivation from a parent structure

If the structure of 4,4 sartorite homologues is strongly idealised a parent structure suggested by Pring (2001) can be defined. This topologically correct parent structure has space group symmetry *Pmnb* and coordinates summarized in Table 6. The *Pmnb* aristotype, or parent structure, goes back to Makovicky (1985) who also derived two further 'subaristotypes', $P2_1/n$ and $P2_12_12_1$ by altering the aristotype via introduction of two possible configurations of pure crankshaft chains. The major reason why this parent structure cannot be stable for the composition $Pb_{16}As_{16}S_{40}$ and a regular *Pmnb* framework is related to the presence of covalent bonds with narrow ranges of 'prescribed' distances and a large Pb : As misfit in size. The bond-strength sums given below illustrate this problem.

The large misfit between the M—S distances required for Pb (Ba) and As (Sb), respectively, in these (except for Ba) highly covalent compounds and the trapezoidal- and crankshaft chain arrangements (see below) are nature's ways to accommodate these disparate polyhedra and requirements in one structure. The covalent As—S and Sb—S distances are pretty 'hard' constrained as shown by Berlepsch et al. (2001). The observed scheme of crankshaft chains and interspaces is a result of accommodation of oriented covalent bonds and lone-electron pairs in conjunction with building blocks constructed of large polyhedra (Pb and/or Ba).

Berlepsch et al. (2001) used the method of bond-length hyperbolae which allowed to distinguish, with good reliability, between 'natural' changes in As—S and Sb—S bond lengths and the 'apparent' bonding schemes from unresolved split cation or ligand positions. This concept (originally defined by Trömel (1981) for Sb^{3+}, Te^{4+}, and I^{5+} bonds with oxygen) is based on the fact that bond pairs $x_n y_n$ of opposing short and long bonds of a single coordination polyhedron of a given cation conform to the hyperbolic correlation $(x_n - a)\,(y_n - a) = c (c > 0)$. However, there exist sometimes other bond pairs lying on linear join (perpendicular to the line $y = x$) between the two branches of a hyperbola. The latter set is interpreted as the result of superimposed and not fully resolved atomic positions indicating that the observed structure is an average.

Figure 3 shows the calculated hyperbolae for the sartorite homologues with the bond-pairs As—S, Ag—S, Pb—S, and Sb—S for rathite (this study) and Sb—S and Ba—S for $Ba_{12}Sb_{18.64}S_{40}$ (Choi and Kanatzidis, 2000) added. As can be seen in Fig. 3 the As—S and Sb—S bond-pairs from the two compounds lay on, or close to, the corresponding hyperbola. As shown by Berlepsch et al. (2001) it is usual that at least one bond-pair formed by (unresolved) ligands around a split cation position is displaced significantly from the corresponding hyperbola (e.g., As5a, As6b or Sb5a, Sb5b in Fig. 3). Ag—S bond-pairs cluster around the line $y = x$ at D_1 (= D_2) values of about 2.8 Å. For Ba—S bond distances a calculated hyperbola is not available. The Ba—S bond pairs exhibit significantly higher values than those for Pb—S and more data are required to establish a regression curve. Bond-pairs for $Ba_{10.48}Pb_{5.52}Sb_{16}S_{40}$ are not shown in Fig. 3 because this structure displays split S positions not directly associated with cation disorder.

Bond-strength sums must be satisfied in the above process, i.e., the 3D network forming arrangements. Highly affected by this is the coordination of S4 (in the parent structure; see below) which bonds to two AsS_3 pyramids of As1 (in *A*4), one PbS_6 octahedron of Pb2 (in *B*4), and two PbS9 tricapped trigonal prisms of Pb1 (in *Z*). Apply-

Table 6. Fractional atomic coordinates of the *Pmnb* ($a = 4.23$, $b = 7.92$, $c = 24.7$ Å) parent structure of 4,4 sartorite homologues and cation and sulfur assignment in the various modulated real structures.

Atom	x/a	y/b	z/c		Rathite	$Ba_{12}Sb_{18.64}S_{40}$	$Ba_{10.48}Pb_{5.52}Sb_{16}S_{40}$	Dufrénoysite
Pb1	0.25	0.2470	0.2956	*Z*	Pb1, Pb2	Ba2, Ba3	Ba5, Ba6, Ba7, Ba8	Pb1, Pb2, Pb3, Pb4
Pb2	0.25	0.9247	0.4289	*B*4	M5, M6	Ba1, Sb5a,b	M1, M2, M3, M4	Pb5, Pb6, As7, Pb8
As1	0.75	0.6593	0.3464	*A*4	M1, M2	Sb1, Sb2	Sb1, Sb2, Sb7, Sb8	As1, As2, As3, As4
As2	0.75	0.3367	0.4474	*C*4	M3, M4	Sb3, Sb4	Sb3, Sb4, Sb5, Sb6	As5, As6, Pb7, As8
S1	0.25	0.1939	0.5097		S9, S10	S9, S10	S9, S10, S11, S12	S6, S7, S8, S9
S2	0.75	0.5122	0.2701		S1, S2	S3, S4	S3, S4, S17, S18	S1, S2, S14, S15,
S3	0.75	0.1398	0.3849		S5, S6	S7, S8	S7, S8, S13, S14	S4, S10, S17, S19
S4	0.25	0.3254	0.1787		S3, S4	S1, S2	S1, S2, S19, S20	S3, S11, S16, S20
S5	0.25	0.4852	0.4077		S7, S8	S5, S6	S15, S16, S5, S6	S5, S12, S13, S18
Ref.				[1]	[2]	[3]	[3]	[4]

[1] labelling scheme for coordination polyhedra in sartorite homologues (Berlepsch et al., 2001);
[2] this study: M1/M2/M4 = As, M3 = (As, Sb), M5 = (Ag, As), M6 = (Pb, As);
[3] Choi and Kanatzidis (2000): M1 = (Ba, Pb), M2–M4 = (Pb, Ba);
[4] Ribár et al. (1969).

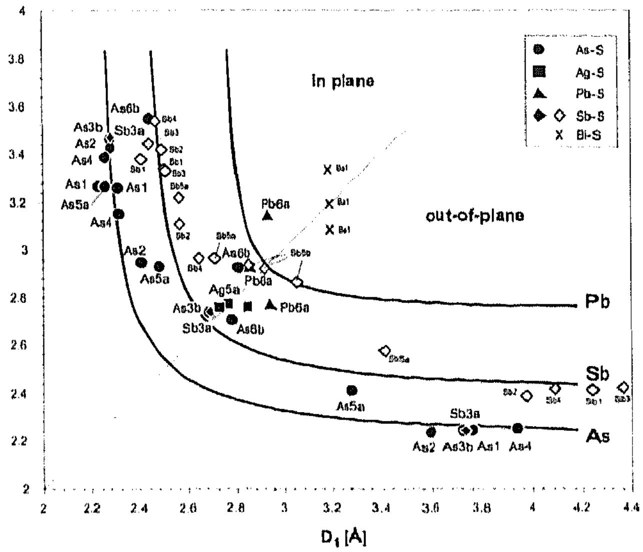

Fig. 3. Calculated element specific bond-length hyperbolae for pairs of opposing bonds taken from Berlepsch et al. (2001) with individual bond-length data of rathite (filled symbols; this study) and $Ba_{12}Sb_{18.64}S_{40}$ (Choi and Kanatzidis, 2000) added. Each pair of bond-lengths consists of a short (x_n) and an opposing long (y_n) M—S bond distance (where $x_n < y_n$ and $n = 1, 2, 3$). $D_1 = x_1, x_2, y_3$ and $D_2 = y_1, y_2, x_3$ defining the points P_1 (x_1,y_1) and P_2 (x_2,y_2) above and P_3 (y_3,x_3) below the median line for each coordination polyhedra.

ing the Pauling bond strength rule (Pauling, 1929) for the calculation of sulfur bond-strength sums ($\sum$ valence/coordination number) 2.78 bond-strength units (bsu) have to be assigned to S4 that is considered strongly overbonded (expected value: 2 bsu). In this approach As^{3+} is treated three-coordinated by S, forming a trigonal pyramid with As^{3+} as apex and three S atoms as base. More powerful bond-valence sum calculations (e.g., Altermatt and Brown, 1985), accounting for variable bond distances, are not considered because of the idealised model character of the *Pmnb* parent structure and unresolved S disorder around split cation positions in the real structures.

In the rathite structure $S4_{Pmnb}$ separates into the symmetry independent sites $S3_r$ and $S4_r$ (Table 6). $S3_r$ is bonded to two AsS_3 pyramids of M1 and M2, two PbS_9 tricapped trigonal prisms of Pb1, and either M5a or M5b. M5 is equivalent to $Pb2_{Pmnb}$ in *B*4 but bonds only to $S3_r$ if it is occupied by Ag^+ (M5a). If M5a is empty and M5b is occupied by As^{3+} it does not develop a bond to $S3_r$. $S4_r$ bonds to one AsS_3 trigonal pyramid of M1, two PbS_9 tricapped trigonal prisms of Pb2, and either to M6b(As) or M6a(Pb). Pauling bond-strength calculations for $S3_r$ yield 2.61 bsu if M5a(Ag) is occupied and 2.44 bsu if M5b(As) is occupied. For $S4_r$ a value of 2.44 bsu is calculated if M6b(As) is occupied and 1.78 bsu if M6a(Pb) is occupied. Overbonding of $S3_r$ is reduced by formation of longer bonds to adjacent As sites of 2.31 and 2.41 Å whereas a normal As—S bond is about 2.25 Å. Note, however, that the former As—S bond-pair involving S3 still sits on and the latter one close to the corresponding hyperbola (Fig. 3). If the partial occupancies are considered the average bond-strength sum for $S3_r$ and $S4_r$ reduces to 2.24 bsu in contrast to 2.78 bsu for $S4_{Pmnb}$ in the parent structure. The above discussion underlines that particularly the heterovalent substitution $Ag^+ + As^{3+} \rightarrow 2Pb^{2+}$ in *B*4 is essential for the stability of the rathite structure (cf. Makovicky, 1985).

A corresponding discussion for the non-stoichiometric compound $Ba_{12}Sb_{18.64}S_{40}$ (Choi and Kanatzidis, 2000), isostructural with rathite, leads to similar conclusions. In addition, Sb5 in *B*4 of $Ba_{12}Sb_{18.64}S_{40}$ is only 66.7% occupied (33.3% vacancies) and Sb5 shows not an As-like bonding scheme of three short bonds but a rather irregular coordination with six Sb—S bond lengths between 2.6 and 3.4 Å. Similar irregular non As-like coordinations are also found in $Ba_{10.48}Pb_{5.52}Sb_{16}S_{40}$ (Choi and Kanatzidis, 2000) for Sb1 and Sb2 (in *A*4) as well as for Sb3, and Sb4 (in *C*4). In general, S overbonding in Sb-rich 4,4 sartorite homologues is reduced by elongated Sb—S bond distances and the hyperbola shown in Fig. 3 may well serve as a basis for predictions.

Dufrénoysite with the same composition as the parent structure displays a different cation arrangement that can easily be understood (Ribár, Nicca and Nowacki, 1969; Fig. 4). The parent structure and dufrénoysite have both Pb in the tricapped trigonal prisms (in *Z*). In addition, in dufrénoysite Pb (on Pb5 and Pb8) is distributed over *B*4 and *C*4 whereas in the parent structure Pb2 occurs in *B*4 only (cf. Table 6). The critical position $S4_{Pmnb}$ in the parent structure separates in dufrénoysite into the symmetry

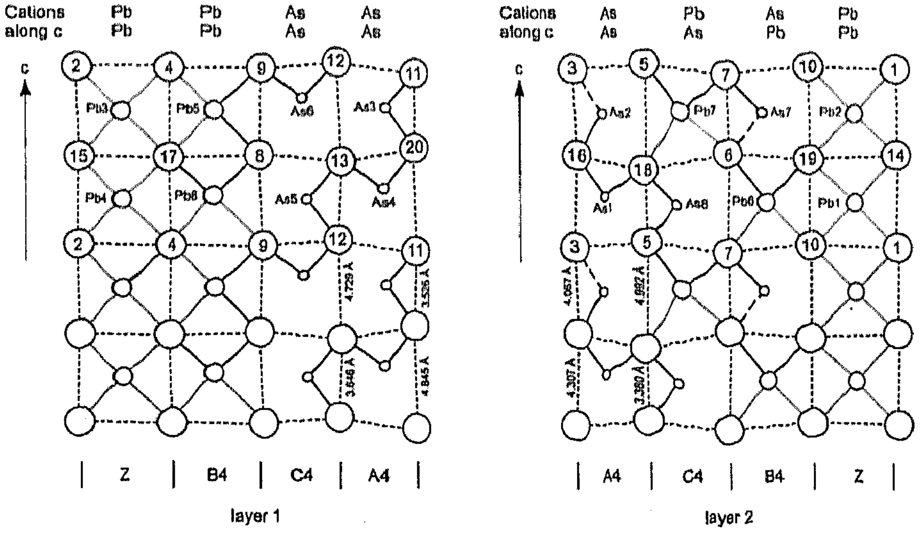

Fig. 4. Symmetry independent $(100)_{SnS}$ layers in dufrénoysite. The dashed fine lines underline the trapezoidal arrangement of the S atoms. Short As—S (and Pb—S) bonds (bold lines) form the crankshaft chains in these layers (see text for details).

independent sites $S3_d$, $S11_d$, $S16_d$, and $S20_d$. The following Pauling bond-strengths sums are calculated for dufrénoysite: $S3_d = 1.78$, $S11_d = 1.78$, $S16_d = 2.78$, $S20_d = 2.44$ bsu. Overbonding of $S16_d$ and $S20_d$ is reduced by enlargement of $S16_d$–As bonds (2.36/2.43 Å) and $S20_d$-As bonds (2.35/2.36 Å). In comparison, the underbonded sites $S3_d$ and $S11_d$ with only one bond to As display bond lengths of 2.18 and 2.22 Å, respectively. The average bond strength sum for $S3_d$, $S11_d$, $S16_d$, and $S20_d$ becomes 2.20 bsu, a value similar to rathite but significantly lower than in the parent structure (2.78 bsu).

All real structures derived from the *Pmnb* parent structure have in common that S positions related to the $S2_{Pmnb}$ are underbonded (1.89 bsu) with only one bond to either As or Sb and four bonds to tricapped trigonal prisms of PbS_9 or BaS_9. This is caused by the sterical environment of $S2_{Pmnb}$ located at a narrow niche on the layers formed by the tricapped trigonal prisms (cf. Berlepsch et al. (2001) for a general discussion of polyhedral volumes of sartorite homologues). The other consequence of this situation is that $As1_{Pmnb}$ (and derived sites) or, in general, *A*4 sites are always occupied by highly charged cations (As^{3+}, Sb^{3+}).

Notice that the poorly refined structure of rathite III of Le Bihan (1962) cannot simply be derived from the *Pmnb* parent structure although the cell dimensions of rathite III are similar to the parent structure with the difference that the *a*-axis of rathite-III is doubled. We consider the structure solution of rathite-III as erroneous.

$(100)_{SnS}$ layers and the role of crankshaft chains

Another approach to the understanding of the differences observed in the structures mentioned above lies in the analysis of the so-called crankshaft chains. Reflecting both an ideal short-long bond distribution as well as the highly covalent character of these structures, an ideal crankshaft chain is an unbroken chain of short M–S bonds in the $(100)_{SnS}$ planes and parallel to $[011]_{SnS}$. In real crystal structures crankshaft chains can be fragmented in various ways and even isolated 'islands' of them exist (Makovicky, 1985).

In the view along the ~8.5 Å period of crystal structures of the sartorite homologues the $(100)_{SnS}$ planes are seen in the projection (Fig. 1). Two such planes form a tightly bonded double layer, i.e., a double layer in which the short M–S bonds (M = As, Sb) perpendicular to $(100)_{SnS}$ are located. Adjacent parallel double layers are separated by the so-called lone-electron pair micelle, i.e., the interspaces that accommodate lone-electron pairs of As (Sb, Pb) in the 'lying' monocapped trigonal prisms (Makovicky, 1985).

In the centrosymmetric structures of rathite and $Ba_{12}Sb_{18.64}S_{40}$ the individual $(100)_{SnS}$ layers of the tightly bonded double layers are symmetry related by inversion centres. In the acentric structures of dufrénoysite and $Ba_{10.48}Pb_{5.52}Sb_{16}S_{40}$ this is not the case; the two layers of a tightly bonded double layer are symmetry independent and they differ in chemical composition. In dufrénoysite and $Ba_{10.48}Pb_{5.52}Sb_{16}S_{40}$ the *c*-glide planes are non-existent and the 2_1 axes have different directions in the two compounds (Table 4). The 2_1 axes in rathite and $Ba_{10.48}Pb_{5.52}Sb_{16}S_{40}$ run parallel to the 7.9 Å translation whereas the 2_1 axes in dufrénoysite run parallel to the 25.7 Å translation. Individual $(100)_{SnS}$ layers of rathite and $Ba_{12}Sb_{18.64}S_{40}$ are shown in Fig. 2 in a comparative way in the view perpendicular to the layer. Selected M–S bonds have been added in order to visualize the crankshaft chains. The above mentioned trigonal MS_3 pyramids (M = As, Sb), commonly observed in sulfosalts when considering only short M–S distances, are completed by additional S atoms out of the displayed $(100)_{SnS}$ plane, i.e., in the adjacent layer within the tightly bonded double layer.

Comparison of the $(100)_{SnS}$ layers of rathite and $Ba_{12}Sb_{18.64}S_{40}$ shows that they have many aspects in common (Fig. 2). In both layers the S atoms show a pronounced trapezoidal arrangement around the (small) cations with an active lone-electron pair (As, Sb). This arrangement changes towards rectangular especially in case of *Z*-type cations (Pb, Ba). Inside these trapezoids the M atoms (M = As, Sb) are bound via short bonds either 'sideways' or 'top/bottom'. In this way the crankshaft chains are formed, a tool that allows an ideal adjustment to the requirements of the various large cations (e.g., Pb, Tl, Ba) incorporated in the crystal structures of the sartorite homologues *sensu largo*.

In both structures (Fig. 2) the large non Z-type cations (M6a in rathite; Ba1 in $Ba_{12}Sb_{18.64}S_{40}$) are located in the same topological *B*4 polyhedron. In rathite, however, the M6 position is a split one. The M5 position is split in both structures (M5a,b *versus* incompletely occupied Sb5a, b). M3 in rathite is also split but the corresponding Sb4 in $Ba_{12}Sb_{18.64}S_{40}$ is not. The crankshaft chains are similar in the two layers, however, in $Ba_{12}Sb_{18.64}S_{40}$ they break up after about $^1/_2$ of the presumed length (Fig. 2), giving Sb_2S_4 groups as in $Ba_{10.48}Pb_{5.52}Sb_{16}S_{40}$. These Sb_2S_4 groups and the surroundings, such as layer 1 in $Ba_{10.48}Pb_{5.52}Sb_{16}S_{40}$, are typical for Sb sulfosalts, as opposed to most As sulfosalts. One exception is, e.g., ramdohrite $Pb_6Ag_3Sb_{11}S_{24}$, as discussed in Makovicky and Mumme (1983). Thus Sb in the Ba–Sb homeotypes of rathite follow the antimony trend (pers. comm. E. Makovicky). Bonds exceeding 2.5 Å (As–S; Figures 4 and 6) or 2.6 Å (Sb–S; Figures 2 and 5), respectively are drawn with dashed lines because the bond lengths are substantially larger than typical As–S and Sb–S should be.

The two (pairs of) symmetry independent $(100)_{SnS}$ layers in the structures of dufrénoysite and $Ba_{10.48}Pb_{5.52}Sb_{16}S_{40}$ are shown in Figs. 4 and 5, respectively. The presence of a larger amount of large cations (Pb, Ba), compared to rathite and $Ba_{12}Sb_{18.64}S_{40}$, disturbs to a certain extent the formation of 'long' crankshaft chains in these layers. However, the crankshafts are still quite well developed in dufrénoysite where the chains are only moderately disturbed by Pb in *B*4 and *C*4 (Fig. 4). The differences between layer 1 and 2 of dufrénoysite are easily seen in Fig. 4. Layer 1 has pure stripes of Pb (in *Z* and *B*4) and As (in *C*4 and *A*4), respectively. In layer 2 this is only true for *Z* and *A*4; *B*4 and *C*4 display a chess-board like alternation of Pb and As positions. Layer 2 is attached to layer 1 in a way that, for instance, As2 forms a trigonal AsS_3 pyramid with S16 and S3 from layer 2 and S15 from layer 1 (Fig. 4). In the so formed tightly bonded double layer the crankshaft chains are oriented at right angle